Journal of Building Engineering 33 (2021) 101593

Contents lists available at ScienceDirect

Journal of Building Engineering

journal homepage: http://www.elsevier.com/locate/jobe

Corrosion resistance of alkali-activated binary reinforced concrete based on natural volcanic pozzolan exposed to chlorides

Ana María Aguirre-Guerrero *, Rafael Andres Robayo-Salazar, Ruby Mejía de Gutiérrez

Composites Materials Group (GMC-CENM), Universidad del Valle, Cali, Colombia

ARTICLE INFO

Keywords:
Alkali-activated concretes
Natural volcanic pozzolan
Chlorides
Steel corrosion
Durability

ABSTRACT

Alkali-activated concretes are being considered as an alternative environmentally friendly construction materials compared to the ordinary Portland cement. However, although these materials have reported mechanical properties comparable to those of OPC, the corrosion of reinforcing bars is a major durability issue that needs to be studied. This article studies the corrosion performance of an alkali-activated binary reinforced concrete (AABC) based on natural volcanic pozzolan (NP) and ground blast furnace slag (GBFS) exposed to chlorides ions. OPC concrete was used as reference material. To carry out the study, accelerated chloride ingress methods (impressed voltage, wet-dry cycles, and saltwater immersion (3.5% NaCl)) were used. Monitoring of the corrosive process was carried out using the techniques of half-cell potential, linear polarization resistance, polarization curves and curves of current intensity versus time. As complementary techniques, surface electrical resistivity and resistance to chloride ion penetration were evaluated. AABC showed higher resistance to chloride ion penetration compared to OPC concrete, a reduction of the charge passed up to 60% at 360 days of exposition. In general, the various accelerated chloride ingress techniques employed in the present research revealed that reinforcing steel embedded in AABCs have a higher resistance to corrosion compared to steel bars embedded in Portland cement (OPC)-based concrete. It should be noted that the B constant values obtained for AABC differ from the values commonly used in (OPC)-based concretes. In addition, the results indicate that the ranges of corrosion probability, such as half-cell potentials or corrosion currents, specified for OPC concretes should be checked for its application in alkali-activated concretes.

1. Introduction

Reinforced concrete based on ordinary Portland cement (OPC) is one of the most widely used materials in the civil industry due to its versatility, properties and low cost. One of the most important factors for the construction industry is the durability, which is determined by the useful life of the material under real service conditions, including its exposure to aggressive environments [1]. Durability is not an intrinsic property of a material, since it depends on the conditions of service, so that in concrete it is known to vary according to the type of environment to which it is exposed. One of the biggest threats that reinforced concrete faces is the corrosion of reinforcing steel due to cracking, delamination, and in severe cases, the partial or total collapse of a structure. The primary cause is the exposition to aggressive environments such as CO_2 and/or the entry of chloride (Cl^-) ions [2–5]. These agents have been responsible for most structural damage and, therefore, a significant increase in investment in structure maintenance and repair. Chloride ions can come from a range of sources - marine environments, the use of de-icing salts (≈NaCl), chemical substances coming into contact with the concrete, or they may be present in the concrete mix, as happens with the inclusion of some types of additives ($CaCl_2$) during production. Chlorides diffuse through the concrete and, on reaching a critical concentration near the steel, cause destruction of the passive layer and initiate the corrosive process, generating pitting corrosion in the steel [6,7].

In addition to concrete durability, a major concern is the environmental impact associated with production, especially relating to the use of Portland cement (OPC). Indeed, the OPC industry generates annually 2 billion tons of CO_2, corresponding to 8–10% of greenhouse gas emissions into the atmosphere [8–10]. For this reason, research applied to the development of alternative low carbon footprint cementitious materials is a priority for the construction sector [11].

* Corresponding author.
E-mail address: ana.aguirre@correounivalle.edu.co (A.M. Aguirre-Guerrero).

https://doi.org/10.1016/j.jobe.2020.101593
Received 13 May 2020; Received in revised form 16 June 2020; Accepted 16 June 2020
Available online 2 July 2020

Among these alternatives, alkali-activated materials (AAMs) have caught attention. These are obtained from chemical interaction between an alumina-silicate material (precursor) and a strongly alkaline solution (activator) [12–14]. AAMs are synthesized at temperatures between 25 and 100 °C, while OPC production temperatures rise to 1460 °C to obtain clinker. AAMs can thus be considered as *potential low carbon cements* [15]. These types of materials also have structural mechanical strengths and physical characteristics such as reduced permeability and thermal stability [16,17].

The precursors commonly used for obtaining AAMs are industrial wastes or by-products such as granulated blast furnace slag and fly ash, as well as thermally activated clays or metakaolin [18,19]. AMMs based on fly ash are the most widely studied, however promoting this type of cement indirectly influences the demand for burning coal, which in turn contributes to the generation of CO_2 into the atmosphere [20]. It has therefore been deemed necessary to seek alternative precursor materials. It is worth noting that recent research has proposed natural pozzolans (NP) of volcanic origin as a sustainable means of obtaining AAM. These are readily available in a number of countries around the world, with no use ever having been made of them in some cases [21], creating strong interest in their use as a precursor of AAMs. The number of studies of NP-based AAMs has grown gradually, emphasizing primarily in the study of mechanical and physical properties [21–28] and reports on durability properties are still few [21,28]. However, no evaluation reports are to be found on the corrosion performance of steel in NP-based alkali-activated concrete (AAC) when exposed to chloride ion-rich environments. Studies of the corrosion performance of reinforcing steel for AACs are limited in general with research focusing mainly on the performance of fly ash/slag-based AAC [29–37]. Generally, researchers have established that different factors influence the corrosive process of reinforcing steel, including precursor type, activator concentration, microstructure, and the types of gels formed as a result of the alkaline activation processes (N-A-S-H; C-A-S-H; C,N-A-S-H) [37,38].

Evaluation has notably already been carried out on the permeability and depth of penetration of chlorides in NP-based AAMs and these properties are linked to susceptibility-to-corrosion of reinforcing steel in these systems. Bondar et al. [39] observed moderate to high chloride permeabilities for NP-based AAC. The authors attribute the results to the high amount of ions present in the pore solution, since these can promote high electrical conductivity when performing the ASTM C1202 rapid chloride permeability test (RCPT), applying 60 V to the system for 6 h. Ghafoori et al. [40] modified RCPT, applying 10V for 6 h and similarly finding a high permeability to chlorides. Najimi et al. [24] used RCPT and rapid chloride migration test (RMT) to assess chloride permeability in NP/slag-based mortars and reported that on increasing slag content from 30 to 50% the depth of chloride penetration was significantly reduced. In another study, Najimi et al. [27] reported that the average depths of chloride penetration are reduced by slightly more than 80% compared to the reference concrete (OPC). It is worth mentioning that for AMMs the transport properties of chloride ions depend on different factors, such as precursor type, the chemistry of the activator solution, the curing regime and the physical and chemical properties of the concrete produced [41]. This makes it challenging to generalize the performance of these materials under attack by chlorides and the consequent corrosion of AAC-embedded reinforcing steel.

Regarding the durability of reinforced concrete, the corrosive processes of steel are slow, sometimes taking years or decades to show problems in concrete structures. Thus, for research studies, different accelerated exposure techniques have been proposed. One of them is impressed voltage technique, which is based on accelerating the diffusion of chloride ions into the concrete matrix through the application of an electric field to the system [42–44]. An advantage of the technique is that in a short time chloride-induced corrosion in the steel bar can be observed. Nevertheless, it is a controversial technique, the application of a voltage to the steel bar could induce an artificial polarization, and the electrochemistry behind the mechanism differs from the natural exposition [45]. Despite this, some authors affirm that it is possible to observe a comparable trend using this quick technique with other accelerated exposure techniques [42,45]. On the other hand, Islam et al. [46] reported a modification to the technique using another anode in the system to do more reliability the results.

Previous studies evaluated the physical-mechanical characteristics of an alkali-activated binary concrete (AABC) based on a mixture of NP and GBFS in proportions of 70% and 30%, respectively, comparing its performance with an OPC reference concrete [26]. The studies reported similar mechanical and physical characteristics for both, further revealing that AABC had a 44.7% lower GWP (global warming potential) than OPC, endorsing it as a low carbon footprint alternative concrete [47]. The carbonation-induced corrosion performance of the reinforced AABC was therefore evaluated, revealing that reinforcing steel remained passive to an accelerated carbonation exposure under controlled conditions (1% CO_2, 65% RH, 25 °C) up to 360 days [48].

Based on the above, the present study aims to evaluate the corrosion performance of a reinforced AABC based on NP (70%) and GBFS (30%) exposed to chlorides (NaCl 3.5%) compared to a 100% Portland cement (OPC)-based reference concrete. To do this, concretes without and with reinforcing steel were made, the former to evaluate chloride permeability and electrical resistivity and the latter to monitor the corrosive process under the accelerated chloride ion ingress techniques of impressed voltage, wet-dry cycles and saltwater immersion (3.5% NaCl). The corrosive process of the reinforcing steel was monitored by electrochemical techniques of polarization curves, linear polarization resistance (LPR) and half-cell potential.

2. Significance of the research

Durability is a key factor, not only as it relates to a set of technical performance properties but from the point of view of sustainability and environmental impact of construction. The more durable the structures are over time, the lower will be the contribution to environmental impacts through the replacement or repair of a structure [2]. As one of the main causes of deterioration, the corrosion of reinforcing steel has emerged as a main research focus due to the economic and social impact involved. As well as, it is important in environmental terms to produce alternative concretes which could contribute less to global warming [11]. Taking into consideration sustainability in construction, a low carbon footprint concrete was produced from alkali-activated NP-based materials, which has been shown similar mechanical properties to OPC concrete [26,47]. Nevertheless, the paucity of studies on the durability of NP-based reinforced AACs, especially in chloride environments, has motivated this study.

Using accelerated techniques for concrete durability assessment, this research work enables a firm appreciation of the performance of reinforced AABC concrete exposed to simulated marine environments at laboratory scale. The results will demonstrate if the concrete might be able to endure exposure to such an aggressive agent and whether it is thus able to replace traditional OPC concrete, in terms of both mechanical performance and durability. Moreover, the use of natural pozzolans of volcanic origin in the production of these alternative concretes is highly encouraged under the principles of environmental sustainability. In addition, the availability of NP in significant quantities in different countries around the world makes this concrete to be considered a viable alternative at industrial scale [21,45].

3. Materials and experimental procedure

Fig. 1 presents the methodology followed in this research.

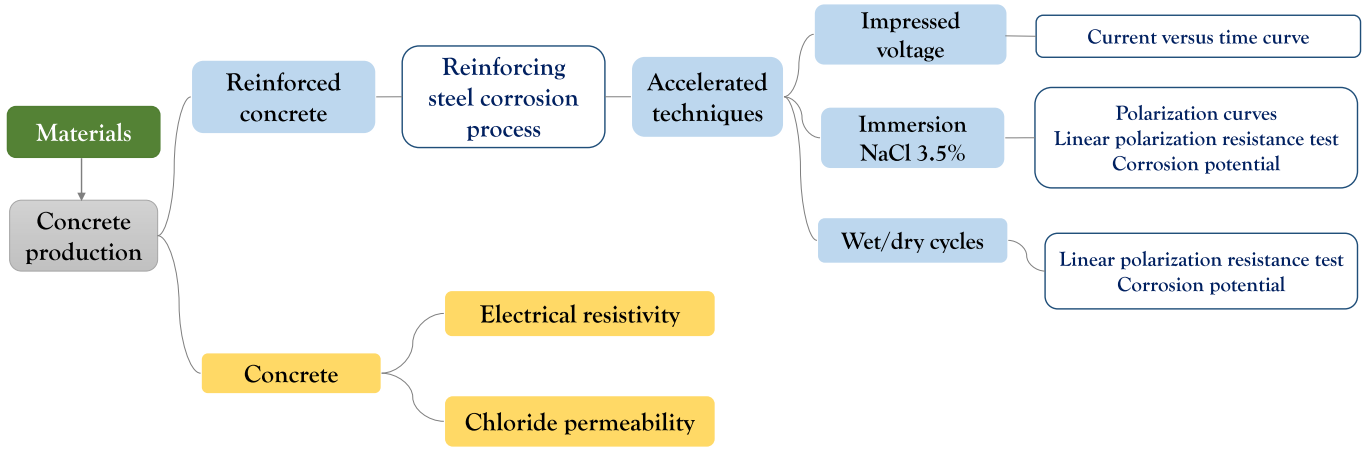

Fig. 1. Experimental methodology.

3.1. Materials

A mixture of natural pozzolan of volcanic origin (NP) and granulated blast furnace slag (GBFS) in a proportion of 70% and 30%, respectively, was used as a precursor to produce AABC concrete. The proportions of the mixture were obtained from a previous study [49]. Additionally, a GU type Portland cement (general use-ASTM C1157 [50]) was employed in the production of the OPC reference concrete. Table 1 reports the chemical compositions of these materials, obtained by X-ray fluorescence (XRF) using a Philips-PANalytical MagiX Pro PW 2440 spectrometer.

As alkaline activator solution, a mixture of industrial grade sodium hydroxide (NaOH) and commercial sodium silicate (waterglass) (Na_2SiO_3: SiO_2 = 32.09%, Na_2O = 11.92%, H_2O = 55.99%), with a solution modulus (SiO_2/Na_2O molar ratio) of 1.1 was used.

Silica sand extracted from a river in the region with a fineness modulus of 1.85 and crushed siliceous gravel of maximum size 12.7 mm were used as aggregates. The ideal granulometric combination of the aggregates (45% sand-55% gravel) was determined based on the Fuller-Thompson method. It is noted that the aggregates meet the standards for use in concrete [51–53].

3.2. Mix designs and specimen preparations

For the design of the AABC and OPC concretes, the following specifications were established: minimum compressive strength of 21MPa after 28 days of curing and slump greater than 18 cm (fluid consistency). To meet these design specifications in AABC concrete, a precursor material quantity (70% NP + 30% GBFS) of 400 kg/m^3 and liquid/solid ratio (L/S) of 0.35 were required. An adaptation of the "absolute volume" method proposed by ACI 211.1 [54] was made for the design of the concrete mix. This same methodology was carried out with the OPC concrete for comparative purposes. Table 2 reports the dry weight dosages for both concretes.

The two types of concrete were produced in a Crete Angle horizontal mixer with 8- and 15-min mixing times for the OPC and AABC concretes, respectively. The mixtures were cast into 76.2 mm diameter and 152.4 mm high metal cylindrical molds and were subsequently vibrated for 30 s on an electric concrete vibrating table to eliminate possible trapped air. The molds were covered for 24 h with a plastic film, after which the cylinders were removed from the mold. OPC and AABC concretes were cured at room temperature (±25 °C) and relative humidity greater than 90%. After 28 days of curing, the compressive strength test was carried out for the two types of concrete. The results are presented in Table 3. The test was carried out in a hydraulic press (ELE International) of 1000 kN capacity, in accordance with the ASTM C39 standard [55]. Specimens of 152.4 mm high and 76.2 mm wide (AABC and OPC without reinforcing steel) after 28 and 360 days of curing were also used to evaluate the electrical resistivity of the concretes.

It should be noted that the porosity properties of concrete are closely linked to the durability performance of the materials. For this reason, Table 3 presents the physical-mechanical characteristics of the concretes at 28 days of curing, which were reported in previous studies [26,48]. The mechanical and porosity characteristics are quite similar. However, OPC concrete has a much more refined pore structure compared to AABC concrete based on what was reported by the mercury porosimetry test. Furthermore, based on the capillary water absorption results, the absorption coefficient K is higher for AABC concretes and the resistance to water penetration m is lower compared to OPC concretes. All of this together corroborates that OPC has a finer pore structure and therefore a greater resistance to water penetration than AABC [48].

To produce the reinforced concrete, a corrugated structural steel bar 150 mm in length and 6.4 mm in diameter was inserted in the

Table 1
Chemical composition of the raw materials (% by weight).

Chemical compound (%)	NP	GBFS	OPC
SiO_2	61.99	37.74	17.99
Al_2O_3	15.52	15.69	3.88
Fe_2O_3	7.33	1.85	4.76
CaO	5.19	40.30	62.28
Na_2O	4.07	0.20	0.23
MgO	2.49	1.30	1.71
K_2O	1.59	0.40	0.32
SO_3	–	–	4.03
LOI[a]	0.48	–	4.14
Others	1.34	2.52	0.66
SiO_2/Al_2O_3 (Molar)	6.79	4.09	–

[a] LOI: Loss on ignition.

Table 2
Concrete mix composition per cubic meter.

AABC concrete		OPC concrete	
Material	Dry weight (kg)	Material	Dry weight (kg)
NP	280.0	OPC	400.0
GBFS	120.0		
Activator	248.9	Water	200.0
Gravel	930.9	Gravel	940.0
Sand	761.6	Sand	769.1
Total	2341.1	Total	2309.1

(Activator: NaOH + *waterglass* + mixing water).

Table 3
Physical-mechanical properties of concretes at 28 days of curing.

Properties	AABC	OPC	Standard
Compressive strength (MPa)	23.11	23.20	ASTM C39 [55]
Indirect tensile strength (MPa)	2.68	2.50	ASTM C496 [56]
Flexural strength (MPa)	4.70	5.94	ASTM C293 [57]
Bulk density (dry) (kg/m^3)	2236	2216	ASTM C642 [58]
Water absorption (%)	5.78	6.99	
Porosity (%)	15.18	15.82	
Porosity by mercury porosimetry			
Total Porosity (%)	15.9	15.5	–
Pore size distribution	Majority pore size 1–10 μm - 6.45% Meso-porosity[a] 3.76%	Majority pore size 0.1–1 μm - 8.6% Meso-porosity[a] 4.99%	–
Water capillary absorption			
Absorption coefficient K (kg/m^{2}s$^{1/2}$)	0.0296	0.0145	SIA 162/1 [59]
Water penetration resistance m (s/m^2) (x10^7)	1.09	4.53	
Effective porosity ε (%)	9.78	9.79	

[a] Meso-porosity: the fraction of pores smaller than 0.1 μm (100 nm).

Table 4
Elemental composition of the structural steel (%).

Chemical element	C	Mn	P	S	Si
Steel rebar	0.30	1.50	0.035	0.045	0.50

centre of each specimen. The chemical composition of the steel is presented in Table 4. The steels were pre-cleaned with acetone to remove possible grease on the surface. The exposure area of the steel bars was delimited with a length of 50 mm, and the rest of the steel bar was coated with corrosion-resistant epoxy paint. Fig. 2 shows the schematic design of the reinforced concretes, which were cured for 28 days at room temperature (25 °C) and relative humidity greater than 90%. Following this, the reinforced concretes were exposed to each of the accelerated chloride ingress techniques to evaluate the corrosive process of the reinforcing steel.

3.3. Accelerated chloride ingress techniques

Because the natural process of diffusion of chlorides in concrete is slow, different techniques such as impressed voltage, wet/dry cycles, and saltwater immersion (3.5% NaCl) were used in this study.

3.3.1. Impressed voltage (IV)

After 28 days of curing, the reinforced concretes (AABC and OPC) were immersed in 3.5% aqueous NaCl solution. Based on the NT Build 356 standard [60], a constant voltage of 5 V was applied, using an external power supply between the anode (steel rebar) and the cathode (stainless steel sheet). Fig. 3 schematically represents the set-up used in the test. The diffusion of the chloride ions was recorded by measuring the current passing through the specimen. The current increases as the chloride ions reach the reinforcing steel, followed by the current continuing to increase until visible cracks, or corrosion products, are observed in the specimens. For the assembly, monitoring and data collection, a U2741A Modular Digital Multimeter was used with an Agilent U2781A chassis and Agilent E3645A DC power supply, ranging from 0 to 35 V/2.2A. Linear polarization resistance (LPR) electrochemical measurements were made before and after performing the IV technique. To carry out the LPR following completion of IV, the system was disconnected and the concrete removed from the aqueous solution and allowed to dry in the laboratory environment (RH:

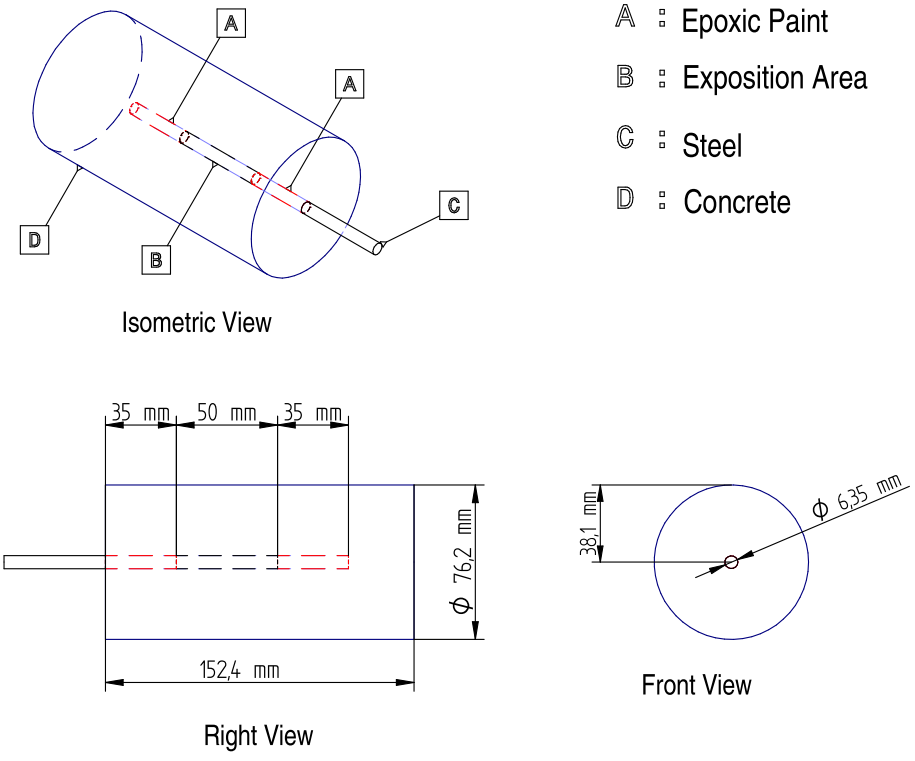

Fig. 2. Schematic view of reinforced concretes.

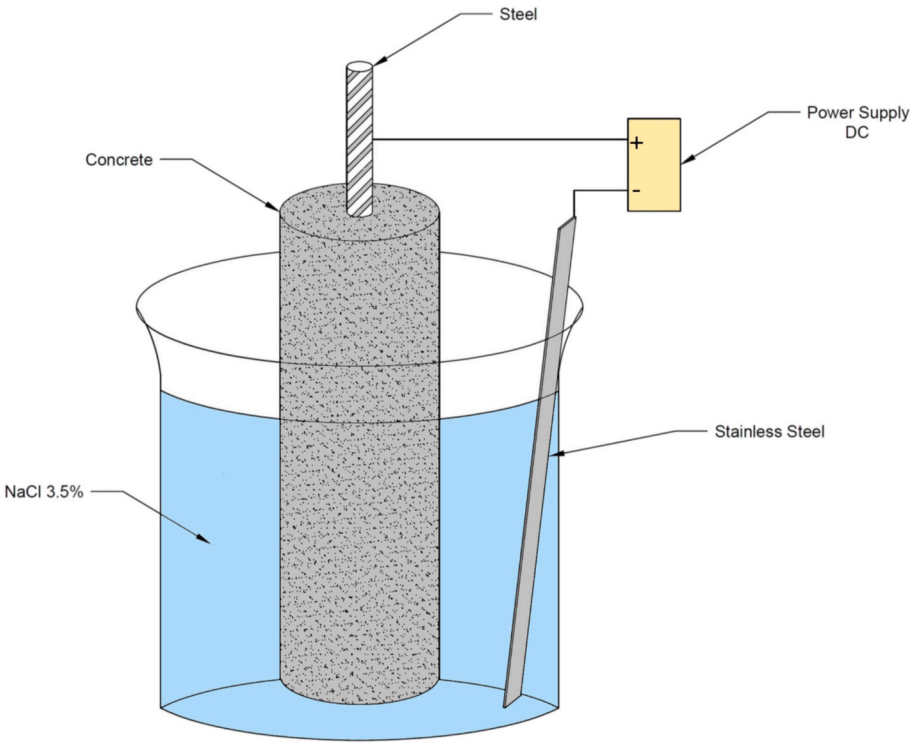

Fig. 3. Schematic of impressed voltage technique.

52.5% and T: 24.8 °C) for 24 h. Two replicated samples were used for each type of concrete.

3.3.2. Wet/dry cycles (w/d)

This technique consisted of exposing the reinforced concretes after 28 days of curing to wet/dry cycles (w/d). Each cycle consisted of one week of immersion in 3.5% NaCl aqueous solution, and the following week under laboratory conditions (RH: 49% and T: 25.3 °C), until 10 cycles were completed. At the end of each cycle, the corrosive process was monitored using the techniques of LPR and half-cell potential. Two replicated samples were used for each type of concrete.

3.3.3. Saltwater immersion (3.5% NaCl)

After 28 days of curing, the AABC and OPC reinforced concretes were exposed to immersion in 3.5% NaCl aqueous solution, the progress of the corrosive process was monitored at 30-day intervals using the LPR and half-cell potential techniques. Likewise, for the determination of the polarization curves, the reinforced concretes were exposed to 600 days of immersion. Different specimens were used for the LPR technique and polarization curves. Two and four replicated samples were used for LPR and polarization curves, respectively.

3.4. Experimental tests

3.4.1. Electrical resistivity

The electrical resistivity of the concrete was determined using the Wenner 4-point method followed in the Spanish standard UNE 83988–2 [61]. The Proceq Resipod Concrete Resistivity Meter was used, with a 38 mm tip spacing. The test was performed in a laboratory environment with a relative humidity (RH) of 44.6% and temperature (T) of 25.4 °C. Three replicated samples were used for each type of concrete.

3.4.2. Rapid chloride permeability test (RCPT)

Since AAMs do not yet have defined standards for evaluating their durability, the accelerated chloride ion permeability test was performed following the procedure described by ASTM C1202 [62] used since 1991 for OPC-based concretes. This test consists of the application of 60 V for 6 h to determine the permeability of the chloride ions in terms of the charge passed through the specimens. The effect of the age of cure of 28 and 360 days in the concretes without reinforcement (AABC and OPC) was evaluated using specimens 50 mm high and 76.2 mm in diameter. Three replicated samples were used for each type of concrete.

3.4.3. Polarization curves

To determine the polarization curves of the reinforcement steels embedded in the AABC and OPC concretes, a three-electrode electrochemical cell was used, featuring a working electrode corresponding to the reinforcing steel, a Ag/AgCl reference electrode Fisher Scientific (4 M KCl saturated) and a counter electrode of stainless steel located around the concrete. Overpotentials from −250 to +250 mV were applied. An Autolab PGSTAT128 N potentiostat/galvanostat was used. After 28 days of curing, the test was conducted for reinforced concrete before immersion (0 days) and after 600 days of immersion in 3.5% aqueous NaCl solution. Through this test, the constant of proportionality B was determined in the passive and active condition of the concrete, according to Equation (1) [63,64].

$$B = \frac{\beta_a \beta_c}{2.303\left(\beta_a + \beta_c\right)} \qquad \text{(Equation 1)}$$

where, β_a and β_c, correspond to the Tafel anodic and cathodic slopes respectively.

3.4.4. Linear polarization resistance (LPR) and half-cell potential tests

The LPR assay was performed under the ASTM G59 standard [65]. A 3-electrode electrochemical cell was used in the same way as in the previous case. Overpotentials from −30 to +30 mV were applied versus the open circuit potential (OCP). An Autolab PGSTAT128 N potentiostat/galvanostat was used. The corrosion rate, i_{corr}, was calculated using the Stern-Geary equation (Equation (2)) [63]:

$$i_{corr} = \frac{B}{R_p} \quad \text{(Equation 2)}$$

where B corresponds to the constant of proportionality calculated from the polarization curves for AABC concrete, and R_p corresponds to the linear polarization resistance. For OPC concretes, the recommended value B = 26 mV was used [66].

The ASTM C876 standard was followed to determine the half-cell potential [67]. A UNI-T UT70A digital multimeter and an Ag/AgCl reference electrode were used.

4. Results and discussion

4.1. Electrical resistivity

The electrical resistivity property is closely linked to the porosity, and thus the durability of the concrete, and mainly with the reinforcing steel corrosion phenomenon because this is due to an electrochemical process. A non-destructive technique, electrical resistivity enjoys wide use in the inspection of reinforced concrete structures as it provides a correlation with the corrosion rate [68]. Fig. 4 shows the electrical resistivity of the AABC and OPC concretes at the age of 28 and 360 days of curing. Lower electrical resistivity values were found for AABC concrete compared to the OPC reference concrete. The RILEM TC-154 committee [66] reports the correlation between the resistivity of the concrete and the corrosion of the reinforcing steel, from which it can be inferred that the AABC concrete at 28 days of curing would have a high probability of corrosion, in contrast to OPC, which would have a moderate such probability. The results presented correlate well with the porosity data presented in Table 3. The OPC has a finer pore structure, so that a tortuous effect on the microstructure offers greater resistance to the flow of charge through the material. After 360 days of curing, the electrical resistivity increases due to the densification of the matrix of both types of concrete. The technique used to measure electrical resistivity, Wenner's four-point method, provides information about the surface electrical resistivity (SER) of the concrete. Table 5 shows the relationship between SER and the chloride ion permeability classification suggested by the Florida Department of Transportation (FDOT) standard for concrete [69]. According to Table 5, AABC would have a probability of high permeability to chloride ions, and OPC a moderate permeability.

The literature reports several studies of electrical resistivity in AAC using the bulk electrical resistivity (BER) method for fly ash/slag-based concrete. Ma et al. [34] recorded a higher BER for a slag-based

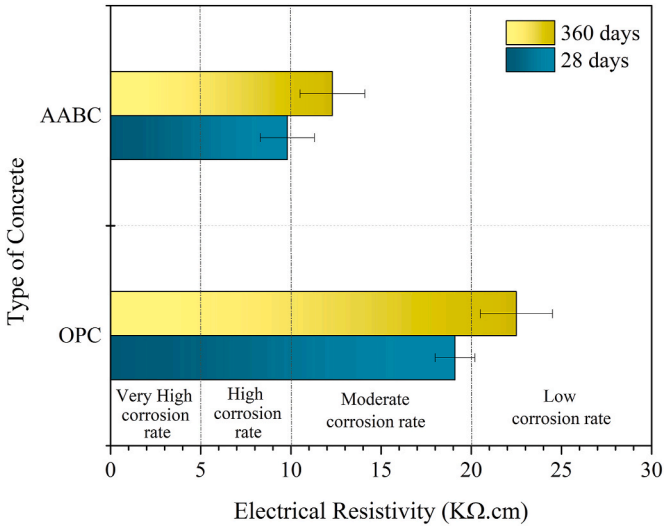

Fig. 4. Electrical resistivity of concretes at 28 and 360 days of curing.

Table 5
Relationship between chloride ion permeability class and surface electrical resistivity (FDOT Standard [49]).

Chloride ion permeability Classification	Surface resistivity test at 28 days (KΩ.cm)
High	<12
Moderate	12–21
Low	21–37
Very Low	37–254
Negligible	>254

AAC, compared to an OPC concrete. The authors attribute the result obtained to the fact that the AAC has a denser, more tortuous pore structure. In contrast, reporting on the electrical resistivity of the pore solution, they observed the slag-based AAC to have a lower electrical resistivity than OPC had, which they attribute to the highly ionic nature of the AAC. The latter may be an important factor that also affects the electrical resistivity values presented in this study, since the SER measurements can be influenced by different factors such as, among others, the ionic nature of the pore solution, humidity, temperature, and pore structure [70]. In recent studies, Cai et al. [71] report that the electrical resistivity of AAM concrete is highly influenced by the concentration of alkali in the system, the precursor type, the replacement of slag in the alkali-activated system, and the curing temperatures. Similarly, Bondar et al. [72] observed that the BER in fly ash/slag-based AAC is influenced by the precursors and the concentrations of the activator solution. To date, there are no reports in the electrical resistivity literature on AAC based on natural pozzolans/slags.

4.2. Rapid chloride permeability test (RCPT)

In order to observe the resistance of the concretes to chloride ion penetration, the RCPT test was performed. Fig. 5 shows the results obtained. The AABC had a much lower charged passed compared to the OPC concrete. According to the ASTM C1202 standard, the AABC concrete has a low permeability to the chloride ion compared to the OPC concrete, which has a high permeability. Researchers such as Bondar at al [39]. and Ghafoori et al. [40] observed high chloride ion permeability for NP-based alkali-activated mortars. However, Najimi et al. [27] observed in NP/slag-based AACs a reduction in chloride ion penetration compared to OPC; the authors state that the chloride migration coefficient is reduced when the percentage of slag used as a sec-

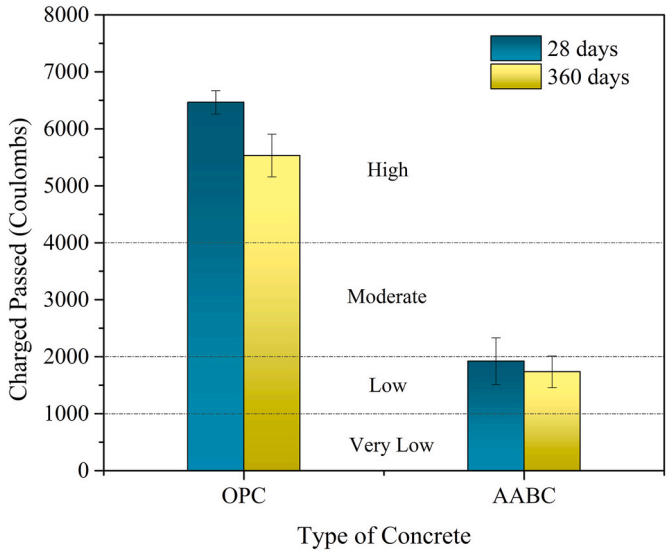

Fig. 5. Rapid chloride permeability test of concretes at 28 and 360 days of curing.

ondary precursor in alkaline activation of binary-type systems increases, corroborating the results of the present study. However, in contrast to the results presented in Table 3 and Fig. 4, it can be deduced that the resistance to chloride ion penetration in AABC does not depend exclusively on the porosity of the material and the electrical resistivity. The transport of chloride ions in AAC therefore depends on several factors, among them the physicochemical characteristics, reaction products (gels) and a possible binding chloride capacity in the concrete matrix [41].

Recent studies have reported that AAMs have chloride ion binding capacity, and it is stated that this depends on the composition of the activator, the type of precursor, the concentration of the chloride solution which they are exposed, and especially the types of gels that are formed in these materials [73–76]. In general, the gels formed are N-A-S-H and/or C-A-S-H type depending on the type of precursor used. Zhang et al. [74] reported that in AAM based on 100% slag, the binding capacity is attributed to the physical adsorption of the C-A-S-H gel, however, the authors observed that if this material is exposed to a high concentration of chloride ions, it is capable of forming the Friedel Salt, whereas if the AAM is of a binary type (fly ash/slag), the capacity of chloride binding increases due to the formation of the N-A-S-H gel, which is generated by the alkaline activation of the fly ash. The binding capacity of the N-A-S-H gel is of the physical adsorption type, since in this the authors did not show Friedel's Salt formation. Regarding AAM based on low calcium fly ash, Noushini et al. [73] also observed a chloride binding capacity, attributing this phenomenon to the adsorption or encapsulation of chloride ions in the pore network of the material. In addition, the authors report the formation of NaCl crystals in the matrix. In the present study, no trials on chloride binding capacity are reported. However, due to the results observed, the behaviour of AABC could be attributed to a possible chloride binding capacity by physical adsorption in its N-A-S-H and C-A-S-H gels (the formation of these gels has been reported in previous studies [49]). Regarding the relationship between chloride permeability and electrical resistivity presented in Table 5, the RCPT results do not agree exactly with the standard FDOT classification.

4.3. Saltwater immersion (3.5% NaCl)

4.3.1. Polarization curves

Fig. 6 shows polarization curves of the reinforcing steel embedded in the AABC and OPC concretes in the passive and active conditions. The passive condition is represented by the curves that have not suffered any exposure to the aggressive environment (0 days) and the active condition is represented by the polarization curves after 600 days of immersion in 3.5% NaCl aqueous solution. Table 6 presents the values of corrosion potentials (E_{corr}) and corrosion currents (i_{corr}), which were obtained by the extrapolation method. The constant of proportionality B was determined by calculating the slopes of the anodic (β_a) and cathodic curve (β_c) (Equation (1)). The RILEM TC154 [66] committee suggests using, for the purposes of calculating the LRP technique, a value of 26 mV for the constant B in the case of OPC-based concrete. According to the experimental results obtained, it was possible to corroborate this suggested value for OPC. As can be seen in Table 6, for the active condition of the reinforcing steel (600 days immersion) embedded in AABC, a value of 17 mV was obtained and 20 mV for the passive condition. Babaee and Castel [29] likewise obtained different B constant values for fly ash/slag binary reinforced concretes to the typical value used for OPC concretes; values of B in the range of 13–20 mV for the passive state and between 45 and 58 mV after 112 days of w/d cycles in NaCl solution (active condition) were reported. These results do not agree with those observed in the present study. This can be attributed to the type of precursors, activators and mixing proportions used in the study, although other parameters related with the electrolyte can also affect the results. These factors could lead to observe differences in the electrochemical behaviour of reinforcing steel embedded in the concrete, due to changes in the composition of the pore solution and microstructure. In general, B might be of a different value in function of alkali-activated system used. According to this, it is necessary to develop a database of B constants based in the experimental results to be used in alkali-activated system [29].

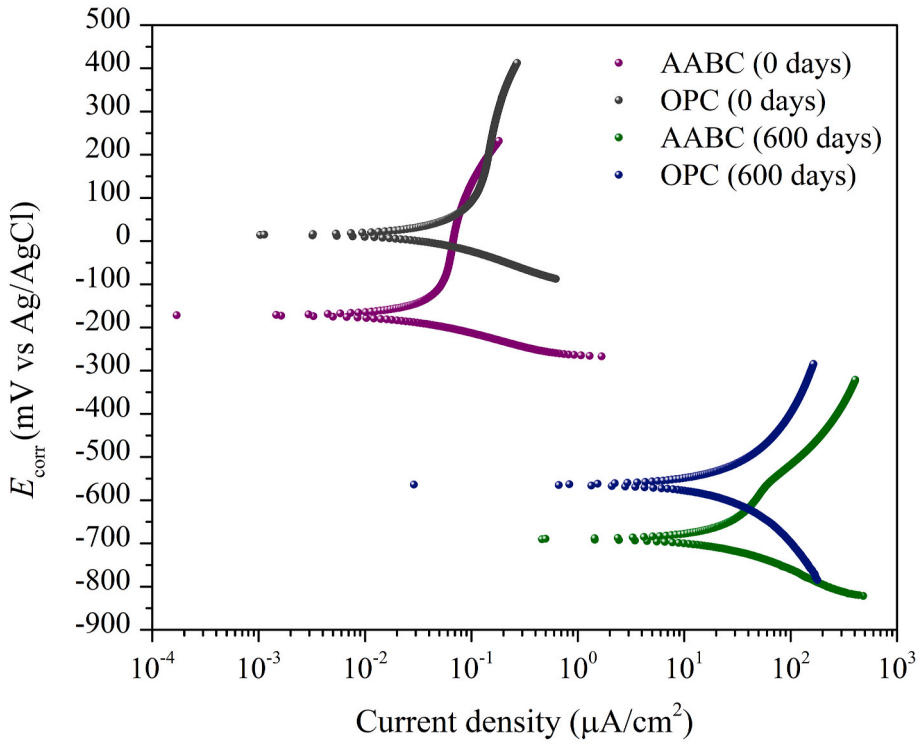

Fig. 6. Polarization curves of reinforcing steel in AABC and OPC concretes 0 days and 600 days of exposition to immersion in NaCl 3.5%.

Table 6
Corrosion potential (E_{corr}), current density (i_{corr}) and constant B calculated using the Tafel extrapolation method.

Concrete	Time of exposition (days)	E_{corr} (mV vs Ag/AgCl)	i_{corr} (μA/cm^2)	B (mV)
AABC	0	−173	0.0294	20.0
	600	−688.27	16.32	17.0
OPC	0	14.9	0.0374	24.5
	600	−563.56	17.60	25.6

It can be seen from the i_{corr} values reported after 600 days of exposure that the steel embedded in AABC shows a decrease in the corrosion rate compared to that in OPC. Meanwhile, the corrosion potential values are much more negative for AABC. This behaviour is attributed to the presence of slag in the alkali-activated binary system. Thus, the sulphide content of GBFS can decrease potential values in redox reactions [77].

4.3.2. Linear polarization resistance (LPR) and half-cell potential tests

Given that the measurements of corrosion potentials (E_{corr}) are considered qualitative and by means of these it is not possible to determine the kinetics of the electrochemical behaviour of the reinforcing steel, Fig. 7 presents the results of both half-cell potential (E_{corr}) and corrosion rate i_{corr}, respectively. Fig. 7a shows E_{corr} of the AABC and OPC concretes exposed to immersion in aqueous 3.5% NaCl solution. According to the electrochemical measurements of potentials, the AABC concrete presents a probability of corrosion greater than 90% from the first days of immersion; moreover, after 120 days of immersion, more negative potentials are observed. OPC concrete presents a probability of corrosion less than 10% in the first days of exposure; after 90 days of exposure the potentials decrease reaching the level of probability of corrosion greater than 90%. In contrast, Fig. 7b shows the corrosion rates (i_{corr}); electrochemical measurements were carried out using the LPR technique. Equation (2) was used to determine i_{corr}. Here, B values of 26 mV and 17 mV were used for the OPC and AABC concretes, respectively. As previously seen, these B values do not match due to the differences in the chemistry and microstructure of both concretes. In the electrochemical behaviour, it can be observed that the reinforcement steel embedded in AABC presents initial corrosion rates in the negligible corrosion level range up to 90 days of exposure. In contrast, in this same time range potentials that indicated high probabilities of corrosion were observed. As mentioned above, the presence of GBFS in AABC concrete induces more negative half-cell potentials. Similar findings have been reported by different researchers; Tennakoon et al. [32] reported for fly ash/slag-based AAC exposed to different concentrations of NaCl very negative potential from the start of exposure compared to their specific OPC reference. These values of potential did not coincide with the actual state of corrosion of the steels. Criado and Provis [77] reported the electrochemical behaviour of reinforced mortars based on the alkaline activation of slag exposed to chloride ions, highlighting very negative potentials and affirming that they are not indicative of the real state of the reinforcing steels. Meanwhile, in fly ash-based AAC, more strongly negative potentials have also been observed without indication of corrosion. Various authors affirm that this could reflect the low concentration of oxygen in the vicinity of the steel and the high rate of formation of the passive layer [36,78].

These results suggest a reconsideration of the ranges of values of probabilities of corrosion for AAC based on half-cell potentials, because different factors may affect the reporting of measurements and comparisons with Portland cement-based concrete (OPC). According to Fig. 7b, after 120 days of exposure the steel is already observed to be in the low corrosion level and i_{corr} values begin increasing and continue to do so until the end of the exposure. Comparing the trend of electrochemical behaviour throughout the exposure time, AABC presents lower corrosion rates compared to OPC concrete, corroborating the results presented in RCPT. OPC-embedded reinforcing steel has a moderate level of corrosion at the end of the exposure, while for AABC the reinforcing steel has a low level of corrosion.

4.4. Impressed voltage (IV)

Fig. 8 presents the curve of current intensity versus time for the AABC and OPC concretes exposed to impressed voltage (IV). In this test, increase in current is related to diffusion through the concrete of chloride ions; a significant increase in current is due to the chlorides reaching the reinforcing steel, initiating the corrosive process and generating corrosion products. These products increase the volume in the vicinity of the reinforcing steel, generating internal tensile stresses in the concrete matrix, leading to cracking and contributing to the deterioration of the concrete [1,2]. When the current reaches its maximum, the corrosion products have already been generated and in some cases, there are already visible cracks in the concrete [79]. As observed in Fig. 8, for the AABC concrete, high current values were

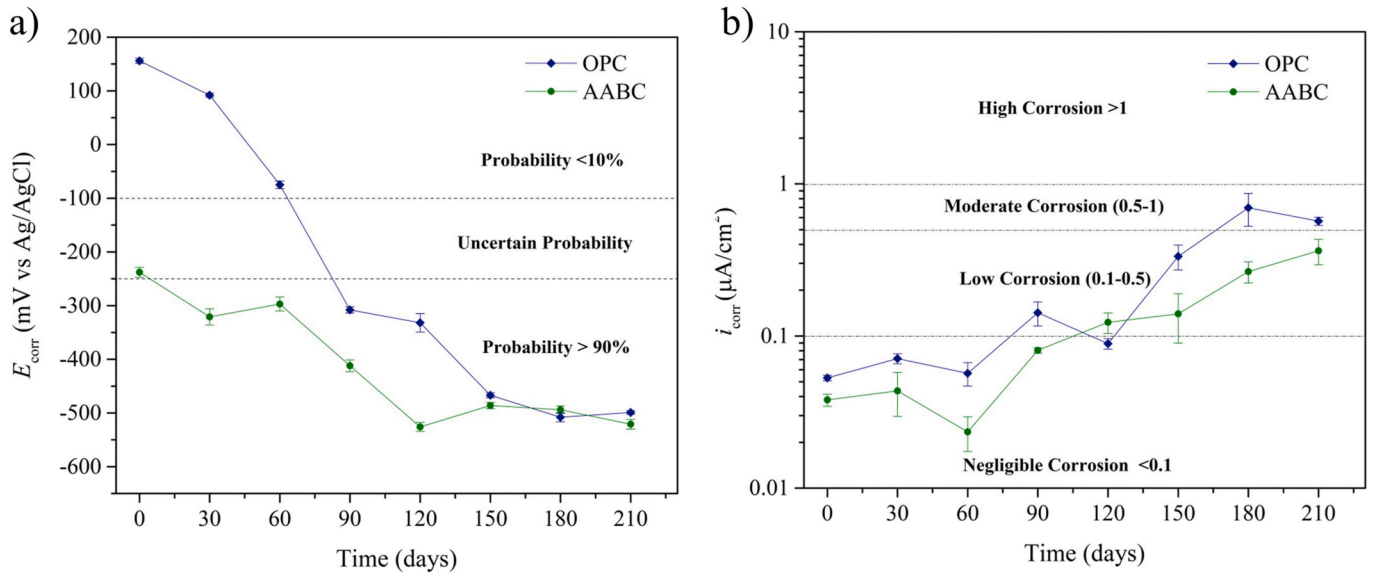

Fig. 7. a) Half-cell potential E_{corr} and b) current density i_{corr} for AABC and OPC concretes exposed to immersion NaCl 3.5%.

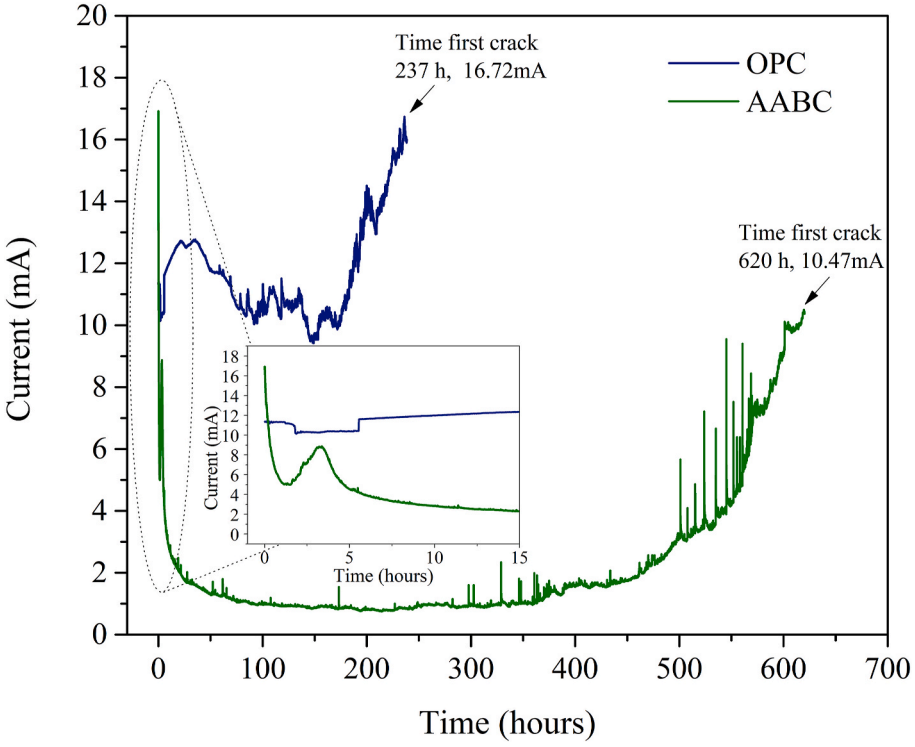

Fig. 8. Current versus time of concretes subject to impressed voltage technique.

recorded at the beginning of the test (0–5 h), reaching a maximum of approximately 17 mA in the first minute, in contrast to the OPC concrete which starts at current values of 11 mA. These initial values corroborate the data observed on electrical resistivity, where AABC presents a lower SER. Likewise, an abrupt drop in current (~5mA) can be observed after the first hour for AABC. Cai et al. [71] reported bulk electrical resistivity measurements for different AAMs. These were found to have unstable values in the initial phase, stabilizing after 2 h. It is possible that the initial data is due to an electrical conductivity influenced by the ionic nature of the material, which generates high initial current values. However, after some time the ionic movement inside the microstructure stabilizes. After 50 h of exposure, the current in AABC drops to ~1 mA and remains stable for up to approximately 400 h. This phenomenon could be attributed to a possible binding of the chloride ions in the gels as a result of alkaline activation, which impedes the passage of charge flow. After 500 h, a remarkable increase in current is observed until reaching its maximum of 10.47 mA at 620 h (~26 days) of exposure for AABC in contrast to OPC, which reaches its maximum of 16.72 mA at 237 h (~10 days). At this point, corrosion products and cracking are observed. AABC concrete significantly increases the time for the appearance of corrosion products and cracks, increasing by a factor of 2.62 the time with respect to OPC. In this regard, similar results have been reported with the use of this technique in fly ash-based AAC, highlighting an increase in the time of appearance of cracks compared to an OPC reference material [80–82].

Fig. 9 presents the i_{corr} values before and after disconnecting the impressed voltage (IV) assay for the AABC and OPC concretes. An increase in corrosion densities can be observed for both concretes after the test. Despite the fact that the AABC concrete remained exposed longer, it reported a lower i_{corr} value than OPC.

Fig. 10 shows the concrete after the IV test, where the presence of a crack is evident for the OPC concrete. However, for AABC, although corrosion products were visualized on the surface, no appreciable crack could be seen with the naked eye. This behaviour could be attributed to the fact that the corrosion products formed on the surface of the steel embedded in AABC do not increase their volume in the same proportion as for the case of those embedded in OPC. This behaviour could be minimizing the effects of cracking and delamination in the structures due to the corrosion of the reinforcing steel in the AABC. Fig. 10 additionally shows the reinforcing steels for both AABC and OPC after IV. Material losses and evident pitting corrosion occur in the two steels due to attack by chlorides.

4.5. Wet/dry cycles (w/d)

Fig. 11 shows the half-cell potentials (E_{corr}) and the corrosion current (i_{corr}) on exposing AABC and OPC concretes to w/d cycles. Fig. 11a shows the electrochemical behaviour of reinforcing steel embedded in AABC, where it is highlighted that the half-cell potentials are more negative compared to OPC from the beginning of the exposure. Meanwhile, from cycle 4 the observed potentials are more negative for the two types of concrete. From Fig. 11b, the i_{corr} corrosion currents are lower for AABC compared to OPC until cycle 7, and from cycle 8 the values of the corrosion rates of the reinforcing steels are closer. However, the trend of a lower i_{corr} for AABC is maintained, corroborating the results presented in chloride permeability.

In the literature, no studies on the corrosion behaviour for AAC based on NP/slag have been reported. However, similar behaviours have been observed in other types of AAC. Tennakoon et al. [32] affirm that in the case of fly ash/slag-based concrete, these presented a low permeability to the chloride ion and also a high resistance to corrosion of the embedded steel compared to an OPC concrete, both exposed to chlorides by immersion. Elsewhere, Babaee and Castel [29] reported, for fly ash/slag reinforced concrete and OPC concrete exposed to w/d cycles in NaCl, similar electrochemical behaviours of the reinforcing steel. In turn, recent research has reported that the passive film that is formed in fly ash/slag-based AAM results in a bilayer-like structure; presenting an inner layer of FeOH and an outer layer rich in FeOOH, due to the high pH of the pore solution, allowing a passive layer with a greater protective capacity to be formed. They also state that on the surface of the passive film, a richly absorbed layer of zeo-

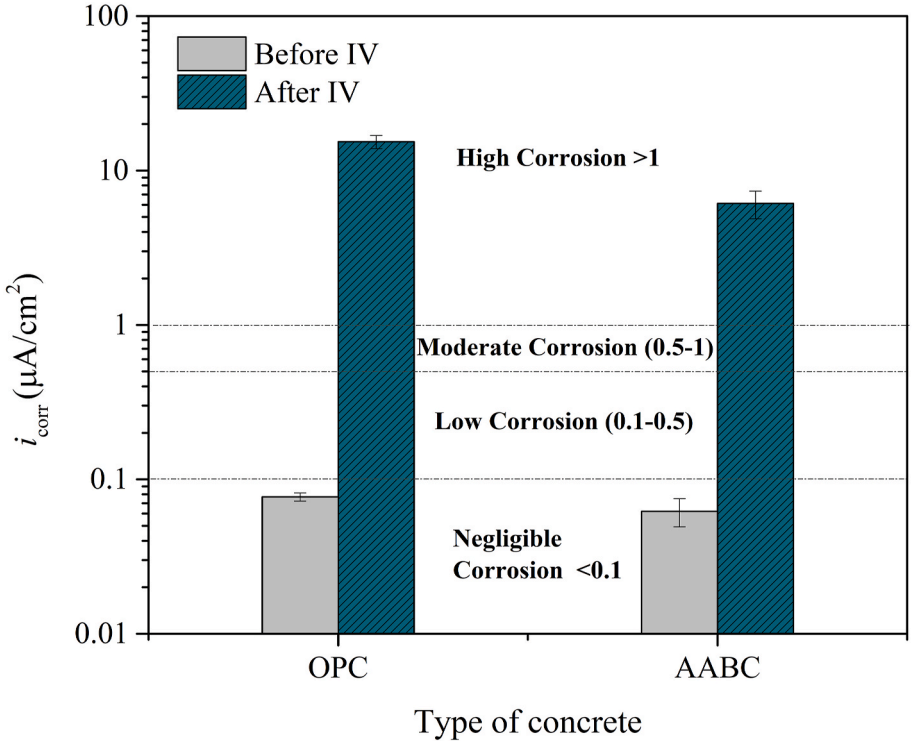

Fig. 9. Current density before and after impressed voltage technique of concretes.

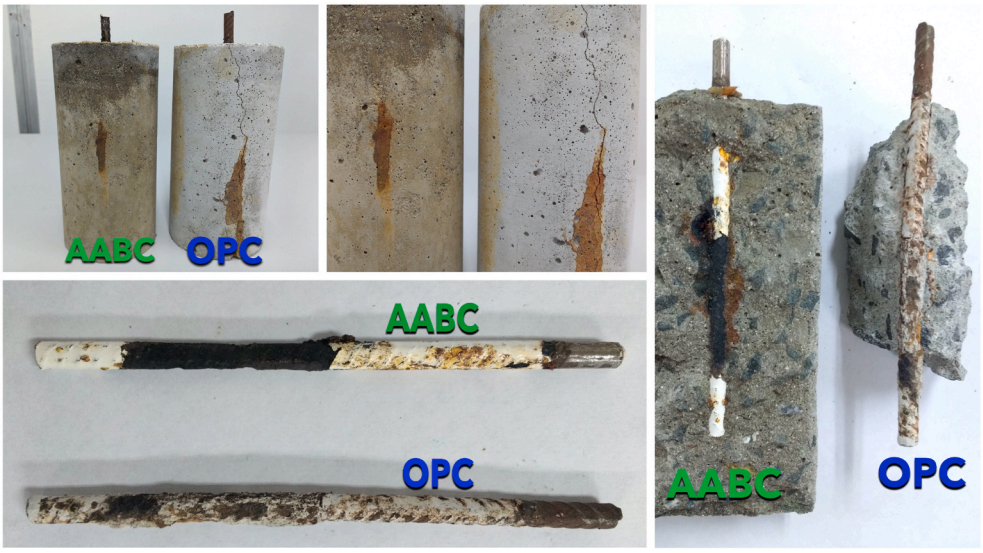

Fig. 10. Visual Inspection of reinforcing steels after IV impressed voltage technique of concretes.

lite-type gels is formed that promotes increased corrosion resistance to reinforcing steel when compared to OPC-based cementitious materials [78,83].

Fig. 12 shows the reinforcing steels after completing exposure to w/d cycles. Steel bars embedded in AABC show less deterioration compared to those embedded in OPC, presenting smaller areas where the phenomenon of pitting is found to be present. The greater protective action of the AABC matrix on the reinforcing steel can be associated with the presence of the layer of alkaline gels present in the vicinity of the steel, which do not allow a rapid spread of chloride ions and therefore less susceptibility to pitting in steel [84]. These findings corroborate the results reported in Fig. 11b. Besides this, a steel embedded in OPC concrete showed crevice corrosion in the interface rebar/epoxy paint, this could influence the corrosion rates. According to Fig. 11b, the standard deviation increases after cycle 6 for OPC concretes. In contrast, the steels embedded in AABC did not show any crevice corrosion.

5. Conclusions

Based on the results, the following conclusions may be drawn:

- Despite having a lower electrical resistivity, AABC has a higher resistance to chloride ion penetration compared to OPC. According to RCPT, AABC reduces charge passed values by 70% and 69%, for 28 and 360 days of curing, respectively. In this sense, the results show that resistance to chloride ion penetration principally depends (even more than on type and level of porosity) on the

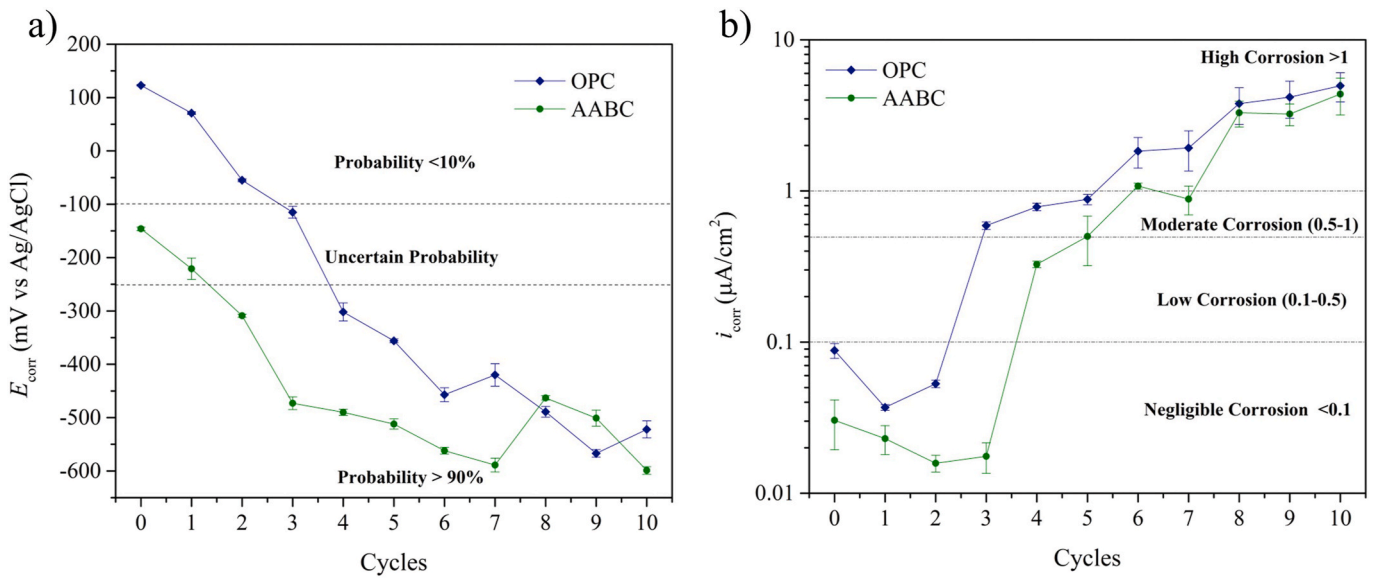

Fig. 11. a) Half-cell potential E_{corr} and b) current density i_{corr} for AABC and OPC concretes exposed to w/d cycles.

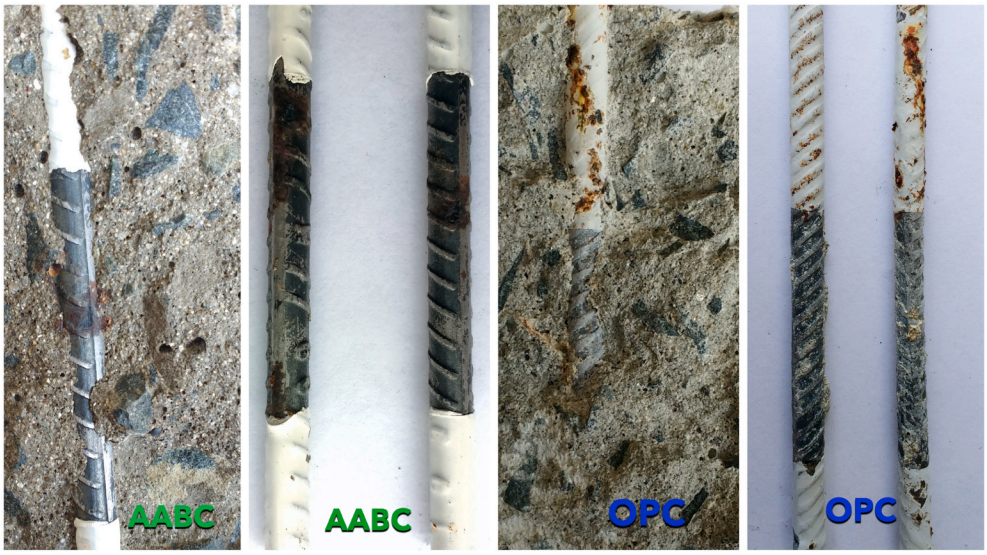

Fig. 12. Visual inspection of reinforcing steel after w/d cycles of concretes.

chemical nature of the gels that are formed in these types of materials, their microstructure and the possible physicochemical binding capacity of the chloride ions within the matrix.

- By means of the polarization curves of four replicates for each concrete, it was possible to determine the constant of proportionality B in the passive and active condition of the steel bars embedded in concrete, in which for the passivation condition of the reinforcing steel in AABC a value of 20 mV was obtained and for the active condition after 600 days of immersion in 3.5% NaCl a value of 17 mV was obtained. These values differ from the theoretical values commonly used in Portland cement (OPC)-based concretes. In this regard, the findings of this research showed that it is not appropriate to assume the same values of B for alkali-activated concretes. Instead, these should be determined experimentally by means of polarization curves.
- At the end of the exposition, the i_{corr} values of w/d cycles were 12 and 8.7 times higher than the values observed in the NaCl immersion, for ABBC and OPC respectively. These suggest that the w/d cycle technique turns out to be more aggressive compared to the 3.5% NaCl immersion technique. The impressed voltage technique led to the observation of cracks due to the corrosion of the reinforcing steel, where the AABC did not suffer a visible crack as OPC did, and the period during which the corrosion products appeared was more than two and a half times longer than for OPC, this being attributed to the microstructure of the gels present in the AABC matrix. In general, the accelerated chloride ingress techniques (impressed voltage, w/d cycles and 3.5% NaCl immersion) employed in the present research revealed that reinforcing steel embedded in NP/slag-based alkali-activated concrete boasts a higher resistance to corrosion compared to steel bars embedded in Portland cement (OPC)-based concrete.

CRediT authorship contribution statement

Ana María Aguirre-Guerrero: Conceptualization, Methodology, Investigation, Validation, Formal analysis, Data curation, Writing - original draft, Visualization, Writing - review & editing. **Rafael Andres Robayo-Salazar:** Conceptualization, Investigation, Formal analysis, Writing - review & editing. **Ruby Mejía de Gutiérrez:** Re-

sources, Writing - review & editing, Supervision, Project administration, Funding acquisition.

Declaration of competing interest

The authors declare that they have no known competing financial interests or personal relationships that could have appeared to influence the work reported in this paper.

Acknowledgements

The authors, members of the Composite Materials Group (GMC), thanks the University of Valle (Cali, Colombia) and the Administrative Department of Science, Technology, and Innovation, COLCIENCIAS for the funding received under contract No. 096–2016. A.M. Aguirre-Guerrero thanks the call No. 784–2017 (COLCIENCIAS-UNIVALLE, SICOP CI 21032), for postdoctoral fellowship in Colombia.

References

[1] A.M. Aguirre, R. Mejía de Gutiérrez, Durability of reinforced concrete exposed to aggressive conditions, Mater. Construcción 63 (2013) 7–38, https://doi.org/10.3989/mc.2013.00313.
[2] M. Alexander, H. Beushausen, Durability, service life prediction, and modelling for reinforced concrete structures – review and critique, Cement Concr. Res. 122 (2019) 17–29, https://doi.org/10.1016/j.cemconres.2019.04.018.
[3] S.W. Tang, Y. Yao, C. Andrade, Z.J. Li, Recent durability studies on concrete structure, Cem. Concr. Res. 78 (2015) 143–154, https://doi.org/10.1016/j.cemconres.2015.05.021.
[4] R. François, S. Laurens, F. Deby, Steel corrosion in reinforced concrete, corros. Its consequences, Reinf. Concr. Struct. (2018) 1–41, https://doi.org/10.1016/b978-1-78548-234-2.50001-9.
[5] O. Anterrieu, B. Giroux, E. Gloaguen, C. Carde, Non-destructive data assimilation as a tool to diagnose corrosion rate in reinforced concrete structures, J. Build. Eng. 23 (2019) 193–206, https://doi.org/10.1016/j.jobe.2019.01.033.
[6] A.M. Aguirre-Guerrero, R. Mejía de Gutiérrez, in: F. Pacheco-Torgal, R.E. Melchers, X. Shi, N. De Belie, K. Van Tittelboom (Eds.), 13 - Assessment of Corrosion Protection Methods for Reinforced Concrete, in: C.I. Sáez (Ed.), Woodhead Publ. Ser. Civ. Struct. Eng., Woodhead Publishing, 2018, pp. 315–353 A.B.T.-E.-E.R. and R. of, https://doi.org/10.1016/B978-0-08-102181-1.00013-7.
[7] X. Shi, N. Xie, K. Fortune, J. Gong, Durability of steel reinforced concrete in chloride environments: an overview, Construct. Build. Mater. 30 (2012) 125–138, https://doi.org/10.1016/j.conbuildmat.2011.12.038.
[8] W. Shen, Y. Liu, B. Yan, J. Wang, P. He, C. Zhou, X. Huo, W. Zhang, G. Xu, Q. Ding, Cement industry of China: driving force, environment impact and sustainable development, Renew. Sustain. Energy Rev. 75 (2017) 618–628, https://doi.org/10.1016/J.RSER.2016.11.033.
[9] B.C. McLellan, R.P. Williams, J. Lay, A. van Riessen, G.D. Corder, Costs and carbon emissions for geopolymer pastes in comparison to ordinary portland cement, J. Clean. Prod. 19 (2011) 1080–1090, https://doi.org/10.1016/j.jclepro.2011.02.010.
[10] L.K. Turner, F.G. Collins, Carbon dioxide equivalent (CO2-e) emissions: a comparison between geopolymer and OPC cement concrete, Construct. Build. Mater. 43 (2013) 125–130, https://doi.org/10.1016/j.conbuildmat.2013.01.023.
[11] R. Maddalena, J.J. Roberts, A. Hamilton, Can Portland cement be replaced by low-carbon alternative materials? A study on the thermal properties and carbon emissions of innovative cements, J. Clean. Prod. 186 (2018) 933–942, https://doi.org/10.1016/j.jclepro.2018.02.138.
[12] J.L. Provis, S.A. Bernal, Geopolymers and related alkali-activated materials, Annu. Rev. Mater. Res. 44 (2014) 299–327, https://doi.org/10.1146/annurev-matsci-070813-113515.
[13] C. Shi, A.F. Jiménez, A. Palomo, New cements for the 21st century: the pursuit of an alternative to Portland cement, Cement Concr. Res. 41 (2011) 750–763, https://doi.org/10.1016/j.cemconres.2011.03.016.
[14] K.H. Yang, J.K. Song, K. Il Song, Assessment of CO 2 reduction of alkali-activated concrete, J. Clean. Prod. 39 (2013) 265–272, https://doi.org/10.1016/j.jclepro.2012.08.001.
[15] A. Naqi, J.G. Jang, Recent progress in green cement technology utilizing low-carbon emission fuels and raw materials: a review, Sustainability 11 (2019) 1–18, https://doi.org/10.3390/su11020537.
[16] Y. Ding, J.G. Dai, C.J. Shi, Mechanical properties of alkali-activated concrete: a state-of-the-art review, Construct. Build. Mater. 127 (2016) 68–79, https://doi.org/10.1016/j.conbuildmat.2016.09.121.
[17] M.M. Hossain, M.R. Karim, M.K. Hossain, M.N. Islam, M.F.M. Zain, Durability of mortar and concrete containing alkali-activated binder with pozzolans: a review, Construct. Build. Mater. 93 (2015) 95–109, https://doi.org/10.1016/j.conbuildmat.2015.05.094.
[18] J.L. Provis, Alkali-activated materials, Cement Concr. Res. 114 (2018) 40–48, https://doi.org/10.1016/j.cemconres.2017.02.009.
[19] Y. Wu, B. Lu, T. Bai, H. Wang, F. Du, Y. Zhang, L. Cai, C. Jiang, W. Wang, Geopolymer, green alkali activated cementitious material: synthesis, applications and challenges, Construct. Build. Mater. 224 (2019) 930–949, https://doi.org/10.1016/j.conbuildmat.2019.07.112.
[20] J. Davidovits, A Continent Is on Fire. STOP Promoting Fly Ash-Based Cements !, Geopolymer Inst., 2020, pp. 1–3, https://doi.org/10.13140/RG.2.2.34889.29283.
[21] R.A. Robayo-Salazar, R. Mejía de Gutiérrez, Natural volcanic pozzolans as an available raw material for alkali-activated materials in the foreseeable future: a review, Construct. Build. Mater. 189 (2018) 109–118, https://doi.org/10.1016/j.conbuildmat.2018.08.174.
[22] C.J.L. Dali Bondar, N.B. Milestone, Alkali-activated natural pozzolan concrete as new construction material, ACI Mater. J. 110 (2013) 331–338, https://doi.org/10.14359/51685667.
[23] M. Najimi, N. Ghafoori, B. Radke, K. Sierra, M.R. Sharbaf, Comparative study of alkali-activated natural Pozzolan and fly ash mortars, J. Mater. Civ. Eng. 30 (2018) 1–9, https://doi.org/10.1061/(ASCE)MT.1943-5533.0002306.
[24] M. Najimi, N. Ghafoori, M. Sharbaf, Alkali-activated natural pozzolan/slag mortars: a parametric study, Construct. Build. Mater. 164 (2018) 625–643, https://doi.org/10.1016/j.conbuildmat.2017.12.222.
[25] R.A. Robayo, R. Mejía De Gutiérrez, M. Gordillo, Natural pozzolan-and granulated blast furnace slag-based binary geopolymers, Mater. Construcción 66 (2016), https://doi.org/10.3989/mc.2016.03615.
[26] R. Robayo-Salazar, R. Mejía De Gutiérrez, F. Puertas, Alkali-activated binary concrete based on a natural pozzolan: physical, mechanical and microstructural characterization, Mater. Construcción 69 (2019), https://doi.org/10.3989/mc.2019.06618.
[27] M. Najimi, N. Ghafoori, Engineering properties of natural pozzolan/slag based alkali-activated concrete, Construct. Build. Mater. 208 (2019) 46–62, https://doi.org/10.1016/j.conbuildmat.2019.02.107.
[28] R. Firdous, D. Stephan, J.N.Y. Djobo, Natural pozzolan based geopolymers: a review on mechanical, microstructural and durability characteristics, Construct. Build. Mater. 190 (2018) 1251–1263, https://doi.org/10.1016/j.conbuildmat.2018.09.191.
[29] M. Babaee, A. Castel, Chloride-induced corrosion of reinforcement in low-calcium fly ash-based geopolymer concrete, Cement Concr. Res. 88 (2016) 96–107, https://doi.org/10.1016/J.CEMCONRES.2016.05.012.
[30] D.M. Bastidas, A. Fernández-Jiménez, A. Palomo, J.A. González, A study on the passive state stability of steel embedded in activated fly ash mortars, Corrosion Sci. 50 (2008) 1058–1065, https://doi.org/10.1016/J.CORSCI.2007.11.016.
[31] M. Babaee, A. Castel, Chloride diffusivity, chloride threshold, and corrosion initiation in reinforced alkali-activated mortars: role of calcium, alkali, and silicate content, Cement Concr. Res. 111 (2018) 56–71, https://doi.org/10.1016/j.cemconres.2018.06.009.
[32] C. Tennakoon, A. Shayan, J.G. Sanjayan, A. Xu, Chloride ingress and steel corrosion in geopolymer concrete based on long term tests, Mater. Des. 116 (2017) 287–299, https://doi.org/10.1016/j.matdes.2016.12.030.
[33] C. Gunasekara, D. Law, S. Bhuiyan, S. Setunge, L. Ward, Chloride induced corrosion in different fly ash based geopolymer concretes, Construct. Build. Mater. 200 (2019) 502–513, https://doi.org/10.1016/j.conbuildmat.2018.12.168.
[34] Q. Ma, S.V. Nanukuttan, P.A.M. Basheer, Y. Bai, C. Yang, Chloride transport and the resulting corrosion of steel bars in alkali activated slag concretes, Mater. Struct. Constr. 49 (2016) 3663–3677, https://doi.org/10.1617/s11527-015-0747-7.
[35] R. Navarro, E.G. Alcocel, I. Sánchez, P. Garcés, E. Zornoza, Corrosion resistance of steel reinforcements embedded in alkali activated ground granulated SiMn slag mortars, Construct. Build. Mater. 230 (2020) 116917, https://doi.org/10.1016/j.conbuildmat.2019.116917.
[36] K.-P. Kunal, A.E. N, Examination of chloride-induced corrosion in reinforced geopolymer concretes, J. Mater. Civ. Eng. 25 (2013) 1465–1476, https://doi.org/10.1061/(ASCE)MT.1943-5533.0000672.
[37] J. Zhang, C. Shi, Z. Zhang, Z. Ou, Durability of alkali-activated materials in aggressive environments: a review on recent studies, Construct. Build. Mater. 152 (2017) 598–613, https://doi.org/10.1016/j.conbuildmat.2017.07.027.
[38] A. Wang, Y. Zheng, Z. Zhang, K. Liu, Y. Li, L. Shi, D. Sun, The Durability of Alkali-Activated Materials in Comparison with Ordinary Portland Cements and Concretes: A Review, Engineering, 2020, https://doi.org/10.1016/j.eng.2019.08.019.
[39] C.J.L.D.B.N.B. Milestone, N. Hassani, Oxygen and chloride permeability of alkali-activated natural pozzolan concrete, ACI Mater. J. 109 (2012) 53–62, https://doi.org/10.14359/51683570.
[40] N. Ghafoori, M. Najimi, B. Radke, Natural Pozzolan-based geopolymers for sustainable construction, Environ. Earth Sci. 75 (2016), https://doi.org/10.1007/s12665-016-5898-5.
[41] J. Osio-Norgaard, J.P. Gevaudan, W. V Srubar, A review of chloride transport in alkali-activated cement paste, mortar, and concrete, Construct. Build. Mater. 186 (2018) 191–206, https://doi.org/10.1016/j.conbuildmat.2018.07.119.
[42] A.M. Sharkawi, A.M. Seyam, Efficiency of accelerated techniques for assessing corrosion protection of blended cements, Mag. Concr. Res. 71 (2019) 637–646, https://doi.org/10.1680/jmacr.17.00269.
[43] Z. Wang, J. Yu, G. Li, M. Zhang, C.K.Y. Leung, Corrosion behavior of steel rebar embedded in hybrid CNTs-OH/polyvinyl alcohol modified concrete under accelerated chloride attack, Cement Concr. Compos. 100 (2019) 120–129, https://doi.org/10.1016/j.cemconcomp.2019.02.013.
[44] S. Hong, F. Zheng, G. Shi, J. Li, X. Luo, F. Xing, L. Tang, B. Dong, Determination of impressed current efficiency during accelerated corrosion of reinforcement, Cement Concr. Compos. 108 (2020) 103536, https://doi.org/10.1016/j.cemconcomp.2020.103536.

[45] S.A. Austin, R. Lyons, M.J. Ing, Electrochemical behavior of steel-reinforced concrete during accelerated corrosion testing, Corrosion 60 (2004) 203–212, https://doi.org/10.5006/1.3287722.
[46] M.A. Islam, B.P. Bergsma, C.M. Hansson, Chloride-induced corrosion behavior of stainless steel and carbon steel reinforcing bars in sound and cracked concrete, Corrosion 69 (2013) 303–312, https://doi.org/10.5006/0706E.
[47] R. Robayo-Salazar, J. Mejía-Arcila, R. Mejía de Gutiérrez, E. Martínez, Life cycle assessment (LCA) of an alkali-activated binary concrete based on natural volcanic pozzolan: a comparative analysis to OPC concrete, Construct. Build. Mater. 176 (2018) 103–111, https://doi.org/10.1016/j.conbuildmat.2018.05.017.
[48] R.A. Robayo-Salazar, A.M. Aguirre-Guerrero, R. Mejía de Gutiérrez, Carbonation-induced corrosion of alkali-activated binary concrete based on natural volcanic pozzolan, Construct. Build. Mater. 232 (2020) 117189, https://doi.org/10.1016/j.conbuildmat.2019.117189.
[49] R.A. Robayo-Salazar, R. Mejía de Gutiérrez, F. Puertas, Study of synergy between a natural volcanic pozzolan and a granulated blast furnace slag in the production of geopolymeric pastes and mortars, Construct. Build. Mater. 157 (2017) 151–160, https://doi.org/10.1016/j.conbuildmat.2017.09.092.
[50] ASTM C1157/C1157M-20, Standard Performance Specification for Hydraulic Cement, ASTM International, West Conshohocken, 2020 PA.
[51] ASTM C136/C136M-19, Standard Test Method for Sieve Analysis of Fine and Coarse Aggregates, ASTM International, West Conshohocken, 2019 PA.
[52] ASTM C127-15, Standard Test Method for Relative Density (Specific Gravity) and Absorption of Coarse Aggregate, ASTM International, West Conshohocken, 2015 PA.
[53] ASTM C128-15, Standard Test Method for Relative Density (Specific Gravity) and Absorption of Fine Aggregate, ASTM International, West Conshohocken, 2015 PA.
[54] ACI Committee 211, 1-91: Standard Practice for Selecting Proportions for Normal, Heavyweight, and Mass Concrete 211 American Concrete Institute, 2002.
[55] ASTM C39/C39M-18, Standard Test Method for Compressive Strength of Cylindrical Concrete Specimens, ASTM International, West Conshohocken, 2018 PA.
[56] ASTM C496/C496M-17, Standard Test Method for Splitting Tensile Strength of Cylindrical Concrete Specimens, ASTM International, West Conshohocken, 2017 PA.
[57] ASTM C293/C293M-16, Standard Test Method for Flexural Strength of Concrete (Using Simple Beam with Center-Point Loading), ASTM International, West Conshohocken, 2016 PA.
[58] ASTM C642-13, Standard Test Method for Density, Absorption, and Voids in Hardened Concrete, ASTM International, West Conshohocken, 2013 PA.
[59] EMPA SIA 162/1, Water Conductivity, Swiss Standard Association, 1989.
[60] NT BUILD 356, Concrete, Repairing Materials and Protective Coating: Embedded Steel Method, Chloride Permeability, Nordtest, 1989.
[61] UNE 83988-2, Concrete durability. Test methods. Determination of the electrical resistivity. Part 2: Four points or Wenner method, Normalización Española, 2014.
[62] ASTM C1202-19, Standard Test Method for Electrical Indication of Concrete's Ability to Resist Chloride Ion Penetration, ASTM International, West Conshohocken, 2019 PA.
[63] ASTM G102-89(2015), Calculation of Corrosion Rates and Related Information from Electrochemical Measurements, ASTM International, West Conshohocken, 2015 PA.
[64] ASTM G3-14, Conventions Applicable to Electrochemical Measurements in Corrosion Testing, ASTM International, West Conshohocken, 2019 PA, 2019.
[65] ASTM G59-97(2014), Standard Test Method for Conducting Potentiodynamic Polarization Resistance Measurements, ASTM International, West Conshohocken, 2014 PA.
[66] RILEM TC 154-EMC, «Electrochemical Techniques for measuring metallic corrosion»: test methods for on-site corrosion rate measurement of steel reinforcement in concrete by means of the polarization resistance method, Mater. Struct. 37 (2004) 623–643, https://doi.org/10.1007/BF02483292.
[67] ASTM C876-15, Standard Test Method for Corrosion Potentials of Uncoated Reinforcing Steel in Concrete, ASTM International, West Conshohocken, 2015 PA.
[68] C.E.T. Balestra, A.Y. Nakano, G. Savaris, R.A. Medeiros-Junior, Reinforcement corrosion risk of marine concrete structures evaluated through electrical resistivity: proposal of parameters based on field structures, Ocean Eng. 187 (2019) 106167, https://doi.org/10.1016/j.oceaneng.2019.106167.
[69] FDOT, Florida method of test for concrete resistivity as an electrical indicator of its permeability, Florida Dep. Transp (2004) 4–7.
[70] P. Azarsa, R. Gupta, Electrical resistivity of concrete for durability evaluation: a review, Ann. Mater. Sci. Eng. (2017) 2017, https://doi.org/10.1155/2017/8453095.
[71] J. Cai, J. Pan, X. Li, J. Tan, J. Li, Electrical resistivity of fly ash and metakaolin based geopolymers, Construct. Build. Mater. 234 (2020) 117868, https://doi.org/10.1016/j.conbuildmat.2019.117868.
[72] D. Bondar, M. Basheer, S. Nanukuttan, Suitability of alkali activated slag/fly ash (AA-GGBS/FA) concretes for chloride environments: characterisation based on mix design and compliance testing, Construct. Build. Mater. 216 (2019) 612–621, https://doi.org/10.1016/j.conbuildmat.2019.05.043.
[73] A. Noushini, A. Castel, J. Aldred, A. Rawal, Chloride diffusion resistance and chloride binding capacity of fly ash-based geopolymer concrete, Cement Concr. Compos. 105 (2020) 103290, https://doi.org/10.1016/j.cemconcomp.2019.04.006.
[74] J. Zhang, C. Shi, Z. Zhang, Chloride binding of alkali-activated slag/fly ash cements, Construct. Build. Mater. 226 (2019) 21–31, https://doi.org/10.1016/j.conbuildmat.2019.07.281.
[75] H. Ye, L. Huang, Z. Chen, Influence of activator composition on the chloride binding capacity of alkali-activated slag, Cement Concr. Compos. 104 (2019) 103368, https://doi.org/10.1016/j.cemconcomp.2019.103368.
[76] M.S.H. Khan, O. Kayali, Chloride binding ability and the onset corrosion threat on alkali-activated GGBFS and binary blend pastes, Eur. J. Environ. Civ. Eng. 22 (2018) 1023–1039, https://doi.org/10.1080/19648189.2016.1230522.
[77] M. Criado, J.L. Provis, Alkali activated slag mortars provide high resistance to chloride-induced corrosion of steel, Front. Mater. 5 (2018) 1–15, https://doi.org/10.3389/fmats.2018.00034.
[78] R. Chen, J. Hu, Y. Ma, W. Guo, H. Huang, J. Wei, S. Yin, Q. Yu, Characterization of the passive film formed on the reinforcement surface in alkali activated fly ash: surface analysis and electrochemical evaluation, Corrosion Sci. (2019) 108393, https://doi.org/10.1016/j.corsci.2019.108393.
[79] E. Güneyisi, T. Özturan, M. Gesoğlu, A study on reinforcement corrosion and related properties of plain and blended cement concretes under different curing conditions, Cement Concr. Compos. 27 (2005) 449–461, https://doi.org/10.1016/j.cemconcomp.2004.05.006.
[80] M. Olivia, H.R. Nikraz, Corrosion performance of embedded steel in fly ash geopolymer concrete by impressed voltage method, Inc. Sustain. Pract. Mech. Struct. Mater. - Proc. 21st Aust. Conf. Mech. Struct. Mater. (2011) 781–786, https://doi.org/10.1201/b10571-141.
[81] Y.-C. Wu, Material Design and Durability Characterization of «non-Brittle» Geopolymer Material, University of Houston, 2015.
[82] F.J.M. Rivera, Strength and Durability of Fly Ash-Based Fiber-Reinforced Geopolymer Concrete in a Simulated Marine Environment, Florida Atlantic University, 2013.
[83] S. Mundra, M. Criado, S.A. Bernal, J.L. Provis, Chloride-induced corrosion of steel rebars in simulated pore solutions of alkali-activated concretes, Cement Concr. Res. 100 (2017) 385–397, https://doi.org/10.1016/j.cemconres.2017.08.006.
[84] J. Shi, J. Ming, W. Sun, Electrochemical performance of reinforcing steel in alkali-activated slag extract in the presence of chlorides, Corrosion Sci. 133 (2018) 288–299, https://doi.org/10.1016/j.corsci.2018.01.043.